ELSEVIER

Biochimica et Biophysica Acta 1369 (1998) 19–33

BIOCHIMICA ET BIOPHYSICA ACTA
BBA

DMSO produces a new subgel phase in DPPC: DSC and X-ray diffraction study

Stephanie Tristram-Nagle [a,*], Tisha Moore [a], Horia I. Petrache [b], John F. Nagle [a,b]

[a] *Department of Biological Sciences, Carnegie Mellon University, 4400 Fifth Avenue, Pittsburgh, PA 15213, USA*
[b] *Department of Physics, Carnegie Mellon University, Pittsburgh, PA 15213, USA*

Received 12 May 1997; accepted 6 August 1997

Abstract

Equilibrium phases and the kinetics of subgel phase transformation of dipalmitoylphosphatidylcholine (DPPC) hydrated with mixtures of dimethylsulfoxide (DMSO)/water have been studied using differential scanning calorimetry (DSC) and X-ray diffraction (XRD). The rate of gel-to-subgel transformation is decreased with a small increase in X, the DMSO/water mole fraction, but then speeds up and becomes faster than in pure water by $X = 0.16$. The DSC scans show multiple subgel peaks, some of which can be attributed to impacted domain growth. For X greater than 0.10, XRD shows that there is a new, stable subgel phase, S, which also accounts for some of the multiplicity of DSC peaks. Our electron density profiles show that the thickness of the bilayer in the S phase is greater than in the usual C subgel phase. We suggest that the S subgel phase is characterized by different headgroup ordering and smaller chain tilt angle than in the C subgel phase. Electron density profiles show that increasing X decreases the water space between bilayers in all phases, subgel, gel and fluid (L_α). For $X = 0.20$, a different gel phase is also observed that may be due to subtle changes in the orientation of chain tilt first observed in partially dehydrated DMPC. The dehydrating effect of DMSO explains the results of a previous study, confirmed in this study, that increasing the concentration of DMSO raises the main transition temperature and eliminates the ripple phase. © 1998 Elsevier Science B.V.

Keywords: Lipid bilayer; Cryoprotectant; Water structure; Domain wall; X-ray diffraction; Differential scanning colorimetry

1. Introduction

Two methods to investigate the structure of phospholipids are: (1) systematic variation of parts of the lipid molecule; and (2) systematic variation of the accompanying solvent. As an example of the first variation, saturated phosphatidylcholines in the normal gel phase exhibit systematic trends in chain tilt and area/molecule with variations in chain length [1,2] and they also exhibit radically new gel phases for longer chain lengths [3,4]. Other investigations have altered the chain unsaturation [5,6], chain asymmetry [7–9], chain branching [10], glycerol backbone chirality [11], linkage between chains and headgroup [12,13] and headgroup substituents [14–16]. Examples of the second variation include dehydration [17–19], hydrostatic pressure [20,21], organic solvents

Abbreviations: DPPC, 1,2-dipalmitoyl-*sn*-glycero-3-phosphatidylcholine; DMSO, dimethylsulfoxide; MLVs, multilamellar vesicles; DSC, differential scanning calorimetry; XRD, X-ray diffraction; X, mole fraction of DMSO/water; T_m, main transition temperature

* Correspondence address. Fax: +1 412-681-0648; E-mail: stn+@andrew.cmu.edu

PII S0005-2736(97)00197-1

[22,23], pH [24,25] and ions [26–29], to vary lipid structure. McIntosh et al. [30,31] mixed glycerol, ethylene glycol or methanol with water and found that the lipid chains interdigitate in these solvents.

In the present study, we have chosen to perturb the water structure by adding increasing amounts of dimethylsulfoxide (DMSO), which is a strongly dipolar molecule with dipole moment nearly $4D$ [32,33] that hydrogen bonds to water molecules more strongly than water hydrogen bonds to itself [34]. The freezing temperature of DMSO/water mixtures decreases to below -70°C at $X = 0.33$ mole fraction of DMSO/H_2O. DMSO also decreases the surface tension of water by as much as $9\,mNm^{-1}$ at $X = 0.3$ [35].

DMSO has been widely used as a cryoprotectant [36–39]. However, it is interesting that the effect of DMSO on the main transition temperature T_m in PCs is different from other cryoprotectants. The T_m of DPPC hydrated with trehalose (a disaccharide) decreased from 42 to 24°C [40] and IR spectroscopy showed direct binding between trehalose and the phosphate moiety of the PC headgroup [41]. Neither glycerol nor ethylene glycol significantly changes T_m with increasing concentration [30]. In contrast, DMSO increases T_m of DMPC multilayers [42]. DMSO also alters the relative stability of different phases. With increasing DMSO concentration, Yu and Quinn showed that the temperature of the pretransition increased more rapidly than T_m so that the ripple phase no longer exists for $X = 0.11$ [43]. We suggest that these phenomena are at least partially related to the dehydrating effect of DMSO that is indicated by electron density profiles obtained from XRD.

The subgel phase in phosphatidylcholines has been much studied [44–48] since its discovery in 1980 by Chen et al. [49]. It is likely that headgroup order is present in the subgel phase [50], which suggests that variation in the solvent will change the subgel structure. Indeed, our diffraction results show that a different subgel phase, with a different headgroup orientation, appears near $X = 0.1$. We suggest that the appearance of this new subgel phase is due to the altered nature of hydrogen bonding in the aqueous solvent when DMSO is added.

The rate of C subgel formation changes dramatically in the presence of DMSO and multiple DSC peaks appear at higher DMSO concentrations. In an earlier work from this laboratory, it was shown that the subgel phase of fully hydrated DPPC forms from the gel phase via a classical nucleation and growth mechanism [51]. Thus, separate domains of the new subgel phase large enough to be detected as a distinct X-ray reflection are produced when the subgel domains are first nucleated at low temperature and then allowed to grow at higher temperatures still below the subtransition temperature. However, when the subgel is formed by simply quenching to a low temperature, the kinetics of its formation are complex [52–54,48], producing multiple DSC peaks and several closely spaced X-ray reflections [51]. Our interpretation of these results was that, under these latter conditions, subgel formation is hampered by collision of growing subgel domains [51,48]; this produces many domain walls and few homogeneous subgel domains. This picture allows us to interpret our complex DSC data in DMSO/water in terms of only two principal subgel phases.

2. Materials and methods

2.1. Sample preparation

2.1.1. Calorimetry

1,2-Dipalmitoyl-*sn*-glycero-3-phosphatidylcholine (DPPC) in lyophilized form was purchased from Avanti Polar Lipids (Alabaster, AL) and used without further purification. The high purity of this lipid was confirmed by thin layer chromatography (TLC) using chloroform : methanol : 7N NH_4OH (46 : 18 : 3, v/v) as the solvent system where $< 0.1\%$ lysolecithin was detected, as well as by the narrow widths (0.14°C) of the main phase transition. Multilamellar vesicles (MLVs) were prepared by first drying DPPC in a vacuum and then hydrating the lyophilized lipid with a DMSO/water solution. DPPC (4.5 mg) was added to the DMSO/water solution (3 g) in 3 ml nalgene vials. These dispersions were cycled three times between 70 and 5°C with 5 min of vortexing at each temperature. Between 6 and 10 samples were prepared at each mole fraction. These samples were then incubated in an ice bath where the sample temperature was 0.3 ± 0.2°C. The mole fractions (X) of DMSO : water were 0.038, 0.10, 0.16, 0.20 and 0.33, which correspond to ratios 1 : 25.3, 1 : 9, 1 : 5.3, 1 : 4

and 1 : 2 DMSO : water molecules, respectively. These samples were vortexed briefly in the cold prior to loading into the calorimeter using a cold syringe. TLC revealed 1% lysolecithin contamination in a 0.1 *X* DMSO/water DPPC sample that had been held at 0.3 ± 0.2°C for six months and then scanned in the calorimeter.

2.1.2. X-ray diffraction

Thin walled 1.0 mm glass capillaries (Charles Supper, Natick, MA) were cleaned by sequentially washing with a chromic acid bath, deionized water, acetone and finally copious amounts of deionized water. After drying with nitrogen the capillaries were flame sealed at one end. Concentrated MLV suspensions, prepared as for DSC except with a solvent to lipid weight ratio of 3 : 1, were loaded into the capillaries using a 1.0 ml Hamilton syringe. In order to remove air bubbles the capillaries were centrifuged for 10 min at 1100 $\times g$ at room temperature. After centrifugation the capillaries were flame-sealed above the water layer and additionally sealed with silicone sealer. Six capillaries with six mole fractions of DMSO/water were loaded into two identical cassettes, and placed into a metal container that was then incubated at 0.3 ± 0.2°C for five months.The cassette was transferred quickly to the cassette holder which was kept at 0°C. Upon completion of the diffraction experiment, the presence of solvent above the lipid suspension confirmed that the sample had not dried out. TLC of these samples that had been X-irradiated for 3–5 days/each revealed the following lysolecithin formation: 0 *X* DMSO – 1%; 0.038 *X* DMSO – 15%; 0.10 *X* DMSO – 10%; 0.16 *X* DMSO – 5%; 0.20 *X* DMSO – 10%; 0.33 *X* DMSO – 1%, when compared to a standard curve. Although the amount of lysolecithin was considerable in some capillaries, the samples were less contaminated when data were taken because they were moved to expose a new position on the capillary before each scan. 0.33 *X* DMSO had a small amount of lysolecithin compared to the other mole fractions since it was X-rayed for only two days.

2.2. Differential scanning calorimetry (DSC)

An MC-2 high sensitivity DSC (Microcal, Northampton, MA) was used. Typical heating scan rates were between 12 and 14°C/h. A Haake compressor was used to cool samples to ca. −1°C before each scan. The MC-2 is interfaced to a PC which uses Microcal software to collect data. Peaks were analyzed using Origin, version 4.1, and the Peak Fitting Module from Microcal Software (Northampton, MA). Enthalpies of all peaks were calculated by comparing their areas to the height of the 8 *X* calibration pulse and then converting to kcal/mol. An example of the use of the Peak Fitting Module is shown in Fig. 1, where a complex DSC peak was best fit by the sum of a Lorentzian (C*) and a Gaussian (C). The specific heat below the subtransition in Fig. 2 has a large slope (ascribed to defects in samples not incubated a long time); use of different kinds of baselines yield at most 20% differences in transition enthalpy [48].

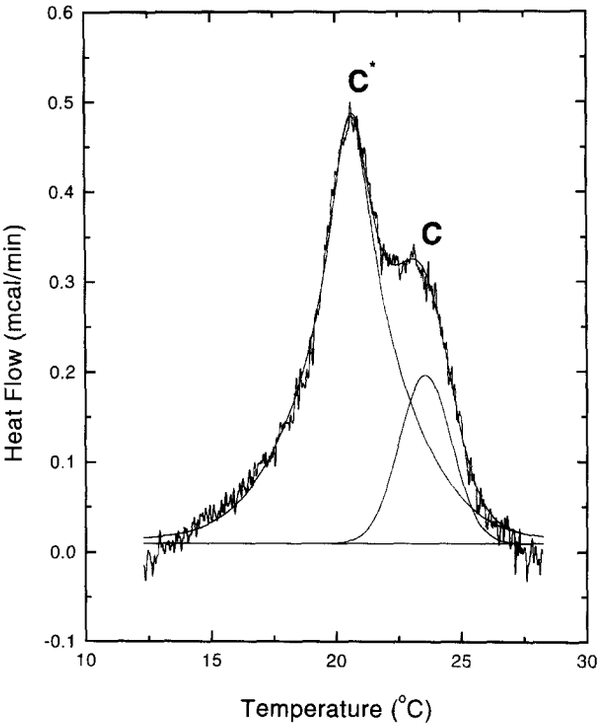

Fig. 1. An example of the enthalpy decomposition of a subtransition using the Peak Fitting Module provided by Microcal Software, Northampton, MA. C* was best fit using a Lorentzian function and C was best fit using a Gaussian function.

2.3. X-ray diffraction

The X-ray source was a Rigaku Microfocus X-Ray Generator operated at 1.4 kW. The sample chamber

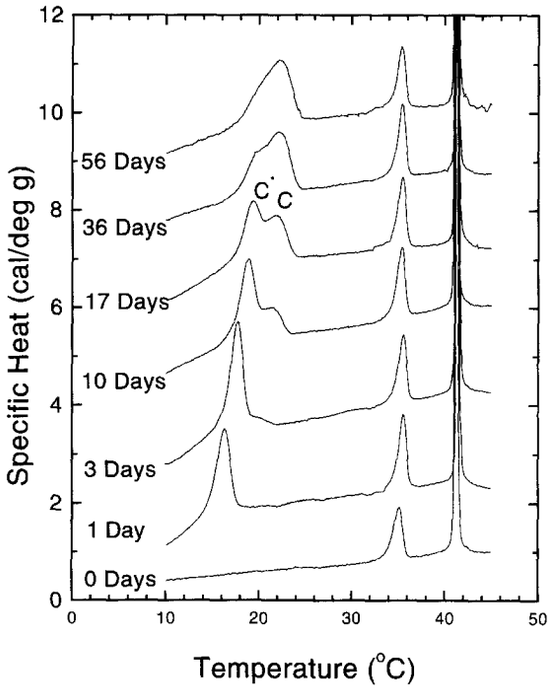

Fig. 2. DSC of DPPC in pure water from Ref. [48]. DPPC was incubated at 0.3 ± 0.2°C for the number of days indicated.

was as in [1]. A swirlcool tube (ITW Vortec, Cincinnati, Ohio) was used to cool the sample container and the temperature was controlled to ± 0.02°C with a Lake Shore DRC-91C Controller using a platinum resistance thermometer and heating strips (Minco Products, Minneapolis, MN). A graphite monochromator selected Cu K_α radiation (λ = 1.542 Å) and defined a beam with angular resolution of full-width at half-maximum $\delta(2\theta)$ (FWHM) = 0.17° in the horizontal direction. The slits before the sample were set to ± 0.75 mm in the horizontal direction and ± 4 mm in the vertical direction. A Bicron scintillation counter was placed horizontally 50 cm after the sample. Evacuated flight paths contained the main beam and the scattered X-rays. Data were collected on each sample for 16–24 h using a step size of (0.05) degrees in 2θ.

Electron density profiles were calculated as follows: The integrated scattering intensity I_h for peaks $h = 1, \cdots, h_{max}$ was obtained using baselines automatically generated by Origin 4.1. The form factors F_h were obtained using the Lorentz correction for powder samples $F_h = \phi_h \sqrt{I_h}\, h$ with the phases ϕ_h = [−, −, +, −, −] as in Refs. [55,56,43]. The electron density function was then calculated as the Fourier transform of the form factors:

$$\rho(z) = C \sum_{h=1}^{h_{max}} F_h \cos\left(\frac{2\pi hz}{D}\right)$$

The interlamellar spacing D was obtained from the highest order of diffraction in order to minimize the error due to slit smear [2]; such errors would systematically reduce D, but by less than 0.3 Å. The zero-order form factor $F(0)$ and the normalization factor C are sample-dependent and were not determined.

3. Results

3.1. Differential scanning calorimetry

When DPPC in water is incubated near 0°C, it slowly forms the subgel phase as shown by the DSC heating scans in Fig. 2. An initial endothermic peak named C * slowly converts into the final subgel peak, named C. Upon rescanning without prolonged low temperature incubation the DSC data are virtually identical to the 0-day scan in Fig. 2, with no subgel peaks and unchanged pretransition and main transition peaks. The presence of the C * peak has been interpreted as due to impaction of many domain walls, since it is not present under conditions where fewer domains are nucleated; such conditions include incubation at 4°C [48] and use of the temperature-jump method [51,57]. As a rough measure of the rates in Fig. 2, we note that at 17 days C * and C have equal enthalpies and the enthalpy of the C subgel peak after 56 days is 4 kcal/mol. The temperatures of all DSC peaks in Figs. 2 and 4–7 are summarized by open symbols in Fig. 3 and the corresponding enthalpies are also shown. The closed symbols for X = 0 show the true equilibrium transition temperatures that are achieved by equilibrium dilatometry [58] or by adiabatic calorimetry [59]. Agreement is good for the main transition and the pretransition; in contrast, for the subtransition equilibration times are long compared to the scanning rate and this elevates the DSC transition temperatures above the true equilibrium transition temperatures [58].

Fig. 4 shows DSC scans for mole fraction X = 0.038, which corresponds to 1 : 25.3 DMSO : water

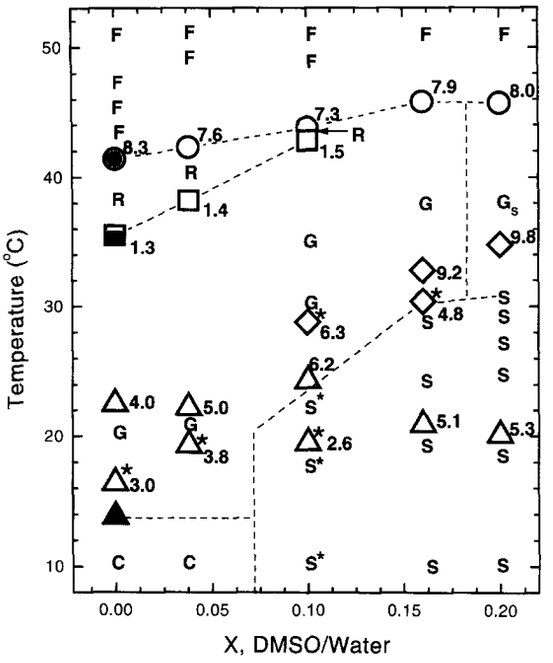

Fig. 3. Rough phase diagram of DPPC in DMSO/water mixtures. The open symbols show temperatures of DSC peaks and the associated numbers show enthalpies in kcal/mole. Subgel data represent the maximum temperature and enthalpy observed for each transition, while pretransition and main transition data represent the average of all the scans at that mole fraction of DMSO. The symbols for DSC peaks indicate: main transition (R → F) (○); pretransition (G → R) (□); usual subgel transition (C → G) (△); second subgel transition (S → G) (◇). The solid symbols at $X = 0$ show equilibrium transition temperatures obtained by dilatometry [74]. The letters show temperatures at which X-ray diffraction found the different equilibrium phases, *F* (fluid), *R* (ripple), *G* (gel), G_S (second gel), *C* (subgel), *S* (second subgel). Domain impacted phases and DSC peaks are indicated by asterisks *. The dashed lines indicate very roughly the regions of phase stability, but each line actually represents a two phase region when $X > 0$ (see text).

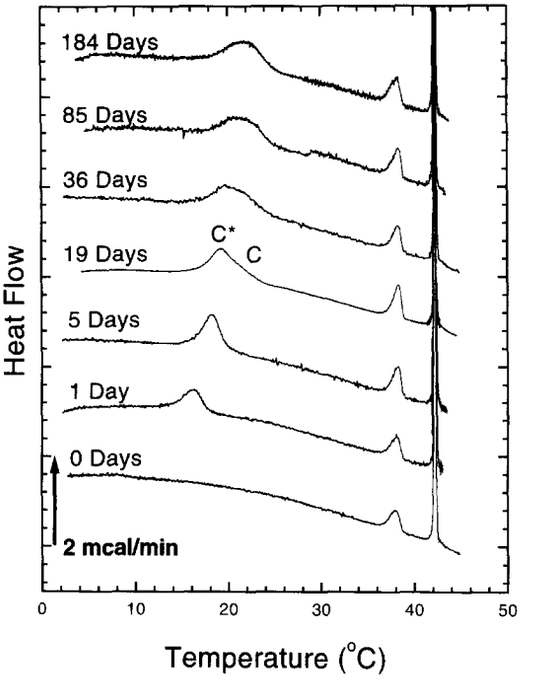

Fig. 4. DSC of DPPC for mole fraction $X = 0.038$ DMSO/water incubated at 0.3 ± 0.2°C for the number of days indicated.

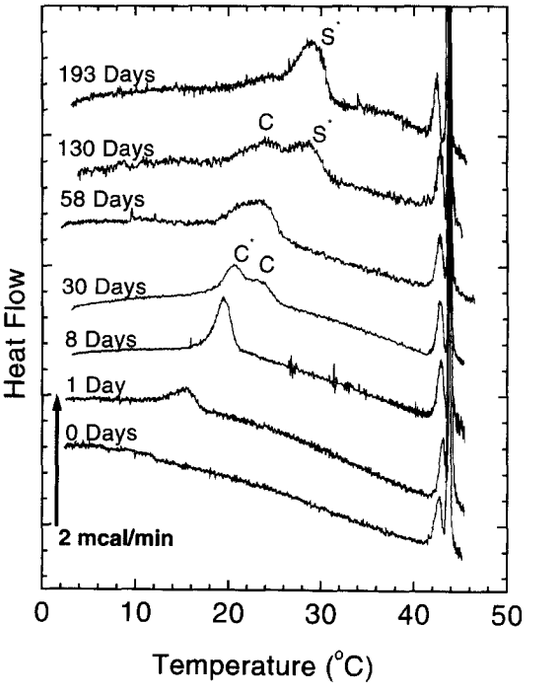

Fig. 5. DSC of DPPC for $X = 0.10$ incubated at 0.3 ± 0.2°C for the number of days indicated.

molecules. The most striking difference from Fig. 2 is that conversion from C* to C is about four times slower than in pure water, with enthalpies of the C* and C peaks that are interpolated to be equal at 66 days. The enthalpies of the pretransition and the main transition do not change significantly from $X = 0$, although the transition temperatures increase as summarized in Fig. 3. As shown in Fig. 5, at the higher mole fraction $X = 0.10$, which corresponds to 1:9 DMSO: water molecules, the pretransition is still present, its enthalpy is slightly increased, and its temperature is shifted upwards to just below that of the main

transition. The conversion between the subgel peaks C* and C is about two times faster than at X = 0.038, but still slower than in pure water, with equal enthalpies of the C* and C peaks at 30 days. However, at 130 days a new DSC peak, named the S* peak, begins to appear while the C peak is still present. The S* peak corresponds to the melting of a new subgel phase as will be shown using X-ray diffraction. The maximum enthalpy of the S* peak for X = 0.10 is 6.3 kcal/mol after 193 days incubation.

DSC scans for X = 0.16, which corresponds to 1:5.3 DMSO:water molecules, are shown in Fig. 6. The main transition has further increased in temperature, although its enthalpy has not changed significantly. However, there is no discernible pretransition and the kinetics of the subgel peaks have changed. Instead of distinguishable C* and C peaks, there is only one peak that we call C that moves to a higher temperature and grows larger (5.1 kcal/mol) in the first nine days. Just as for X = 0.10, for X = 0.16 the C peak eventually vanishes at long incubation times and two new peaks appear. We call the peak that persists at long times S. The S peak is the only

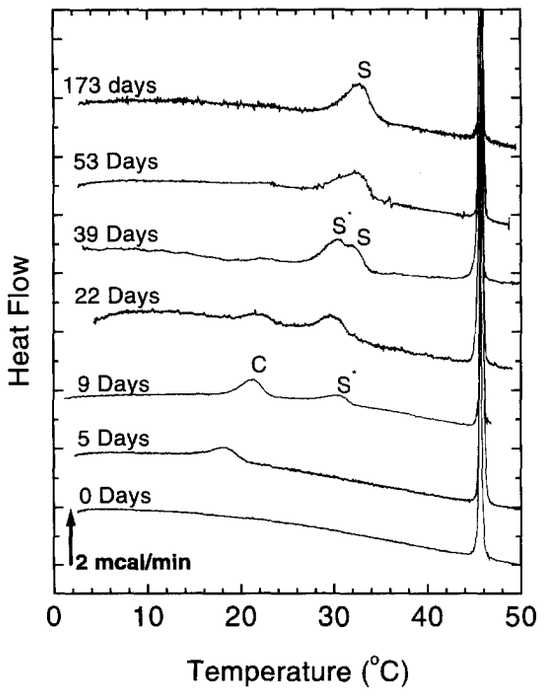

Fig. 6. DSC of DPPC for X = 0.16 incubated at 0.3 ± 0.2°C for the number of days indicated.

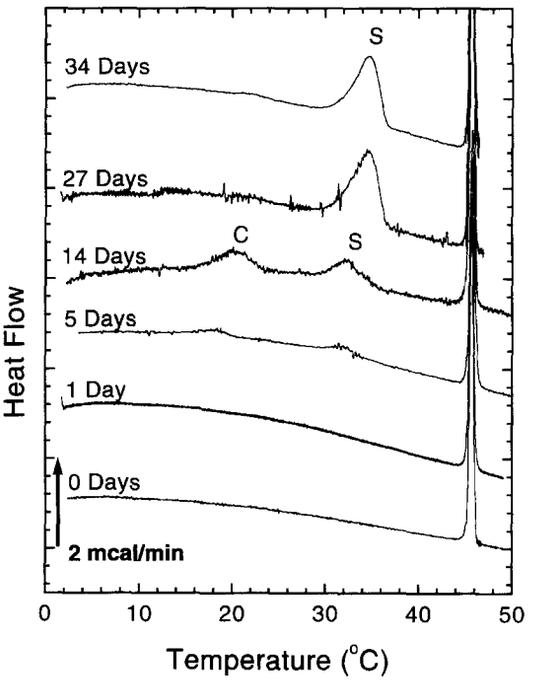

Fig. 7. DSC of DPPC for X = 0.20 incubated at 0.3 ± 0.2°C for the number of days indicated.

peak present at 173 days incubation. The maximum enthalpy of the S peak (9.2 kcal/mol) is even larger than that of the main transition (7.9 kcal/mol). We interpret the S* peak as a metastable transient due to impacted domains in analogy to the interpretation of the C* and C peaks that appear for smaller values of X. It may be noted that DSC alone cannot indicate whether the C peak for X = 0.16 is more analogous to the C or the C* peaks that occur for smaller X. Similarly, DSC cannot indicate whether the peak at X = 0.10 that persists at long times is more analogous to the S* or the S peak for X = 0.16; more support for this identification will come from XRD.

At X = 0.20, or 1:4 DMSO:water molecules, the kinetics of formation of both the C peak and the S peak are quite rapid, as shown in Fig. 7. At 14 days incubation, the enthalpy of the C peak is 5.3 kcal/mol, but by 27 days this peak completely disappears. The enthalpy of the S peak is already 4.7 kcal/mol at only 14 days and by 27 days it has grown to 9.6 kcal/mol. At 27 days transformation into the S phase appears to be complete, since there is no further change in the DSC scan at 34 days.

When the concentration of DMSO/water is increased further to X = 0.33, which is 1:2

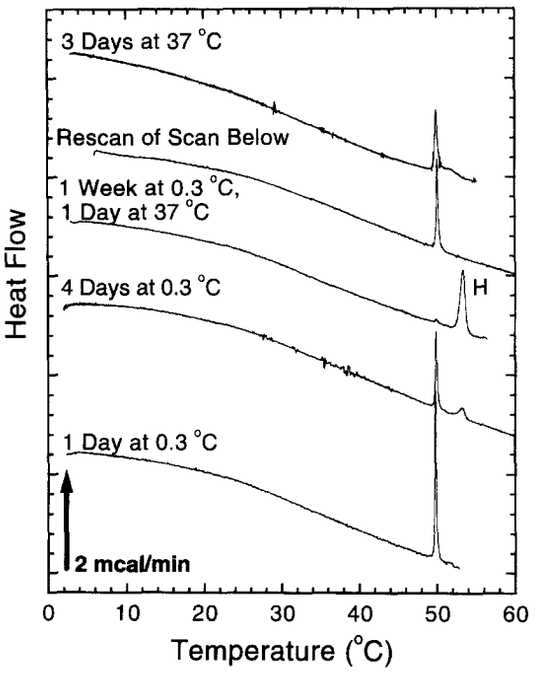

Fig. 8. DSC of DPPC for $X = 0.33$ incubated as indicated.

DMSO : water molecules, the phase behavior is radically different as shown in Fig. 8. The only remaining DSC peak near 50 °C might be supposed to be a 'main transition,' but it has an enthalpy of only 1.5 kcal/mol. When the sample is incubated for four days at 0.3 ± 0.2°C, this 'main transition' is reduced and a new peak begins to grow near 52°C. In analogy to the phase behavior of dimyristoylphosphatidylethanolamine [60], this new peak might be described as a 'subgel' peak which melts above the main transition and which would indicate that the gel phase is metastable at all temperatures. We call this peak H, for high-temperature melting peak. The enthalpy of the H peak increased to 1.5 kcal/mol when the sample was held for one day at 37°C after a one week nucleation at 0.3 ± 0.2°C. When this sample was recooled to 0°C and rescanned, this peak vanished and the small main transition reappeared. Holding the sample at 37°C, apparently, allows already nucleated domains to grow more rapidly, but domains will not nucleate at this higher temperature because the H peak did not appear when the low temperature step was omitted and the sample was just held for three days at 37°C.

3.2. X-ray diffraction

X-ray scattering for $X = 0.33$ showed no evidence of bilayers or any other ordered lipid phase over the temperature range of 10 to 56°C. Almost all the scattering from this sample was near $2\theta = 0$, suggesting that this is an amorphous material. Thus, the transitions seen by calorimetry at 49.8 and 53.3°C were not correlated with a detectable structural change. This sample was also colorless in appearance which is different from the DPPC samples at all other mole fractions of DMSO which appeared opaquely white.

Samples that had incubated for five months at 0.3 ± 0.2°C were carefully transferred to the diffractometer at low temperature and X-ray spectra were first taken at low temperatures to detect subgel phases. Representative spectra, normalized to the height of the first-order lamellar peak, are shown in Fig. 9.

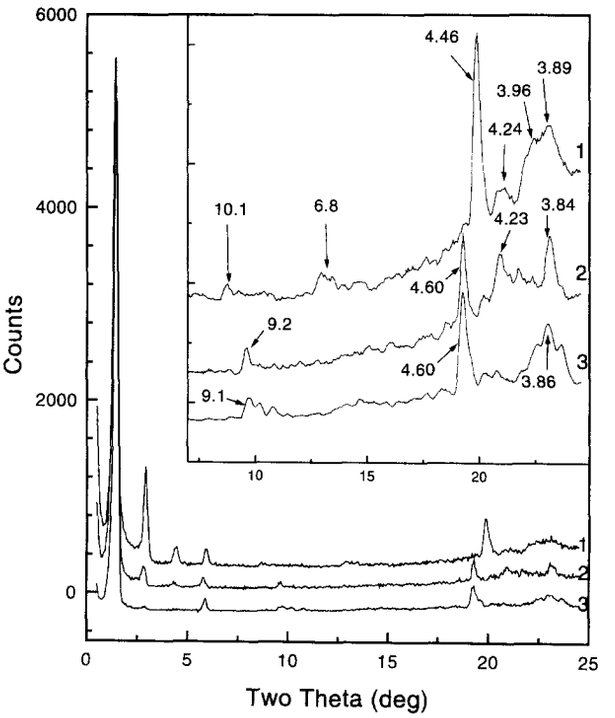

Fig. 9. Subgel phase XRD spectra of DPPC samples incubated for five months at 0.3 ± 0.2°C at the following DMSO/water mole fractions X and temperatures: (1) $X = 0$, 10°C; (2) $X = 0.10$, 20°C; (3) $X = 0.20$, 20°C. Spectra are offset along the vertical axis for clarity.

Table 1
Observed and calculated spacings in Angstroms

X	T (°C)	Phase	D_{LA}	D_{HH}	D'_W	D_{IA}	D_{WA}
0	10	C	59.3	42	7.3	10.1, 6.8	4.46, 4.24, 3.96, 3.89
0.038	10	C	58.8	42.7	6.1	10.2, 6.9, 6.5	4.46, 4.23, 3.99, 3.88
0.10	20	S^*	61.1	44.9	6.2	9.2	4.60, 4.23, 3.84
0.16	20	S	60.5	46.4	4.1	9.1	4.60, 4.26, 3.85
0.20	20	S	60.1	46.2	3.9	9.1, 8.7, 8.2	4.60, 3.94, 3.86, 3.76
0	20	Gel	63.8	44.2	9.6		4.25, 4.15
0.038	20	Gel	62.4	44.2	8.2		4.25, 4.14
0.10	35	Gel	62.2	44.2	8.0		4.26, 4.11
0.16	38	Gel	60.2	44.1	6.1		4.26, 4.12
0.20	38	Gel	59.9	44.3	5.6		4.37, 4.26, 3.13
0	38	Ripple	69.7				4.24
0.10	43	Ripple	69.5				4.26
0	51	Fluid	67.3	38.7	18.6		4.6 (broad)
0.10	51	Fluid	62.0	40.6	11.4		4.6 (broad)
0.16	51	Fluid	54.4	36.9	7.5		4.6 (broad)
0.20	51	Fluid	53.5	38.6	4.9		4.6 (broad)

Abbreviations: LA – low angle; IA – intermediate angle; WA – wide angle; HH – head-to-head; W′ — water. $D'_W = D_{LA} - D_{HH} - 10$ Å.

Spectrum 1 for DPPC in pure water ($X = 0$) exhibits a typical subgel pattern characterized by several well-identified peaks in the intermediate-angle region (7–17°C) as well as several wide-angle peaks in the region 17–24°C. The low-angle lamellar peaks give the typical subgel interlamellar spacing of 59.3 Å. The spectrum at $X = 0.038$ (not shown) was very similar to spectrum 1 in Fig. 9. The phase that produces these spectra will be called C in this paper. All D-spacings are summarized in Table 1. The letters in Fig. 3 show the temperatures and mole fractions X at which the different phases were observed by X-ray diffraction.

Spectrum 3 in Fig. 9 is for $X = 0.20$ at 20°C. The presence of the peaks in the intermediate-angle region near $2\theta = 10°$ and the large separation of the two main peaks in the wide angle region distinguishes this from any gel phase. It is equally clear from Fig. 9 that this spectrum is quite different from the usual C subgel phase in DPPC. We interpret spectrum 3 as a new subgel phase which we will call S. An identical spectrum was obtained at 30°C and then at 10°C indicating that the S phase is stable between 10 and 30°C. The spectrum for $X = 0.16$ is nearly identical to spectrum 3 except that its features are less sharp (data not shown). All D-spacings are summarized in Table 1. Fig. 3 shows the temperatures and mole fractions X at which the different phases were observed by X-ray diffraction.

Upon initial loading of the $X = 0.10$ sample at 10°C, phase coexistence of two phases with D-spacings 55.3 and 61.1 Å was observed. Upon raising the temperature to 20°C, only the larger D-spacing persisted. We interpret this as the melting out of the C phase. The spectrum of the remaining phase is spectrum 2 in Fig. 9. It is clear that spectrum 2 is much more similar in both the wide-angle region and the intermediate-angle region to the S phase spectrum 3 than it is to the C phase spectrum 1 in Fig. 9. We, therefore, identify this as an S-type phase. There are, however, differences between spectra 2 and 3. Because of these differences, we suggest that spectrum 2 belongs to a domain impacted S phase that we call S^* and this accounts for our identification of the DSC peak in Fig. 5 as being an S^* peak.

In Fig. 10 we turn to gel phase X-ray spectra. Spectrum 1 is the typical gel phase pattern for DPPC ($X = 0$) at 20°C with five orders in the low angle region and a sharp (2,0) wide-angle peak at 4.25 Å with a broader (1,1) peak at 4.15 Å. The spectra at $X = 0.038$ and 0.10 were qualitatively very similar; the main difference was smaller low-angle D-spacings (Table 1). Spectrum 2, obtained for $X = 0.16$ at 38°C, is also similar to the usual gel phase spectrum

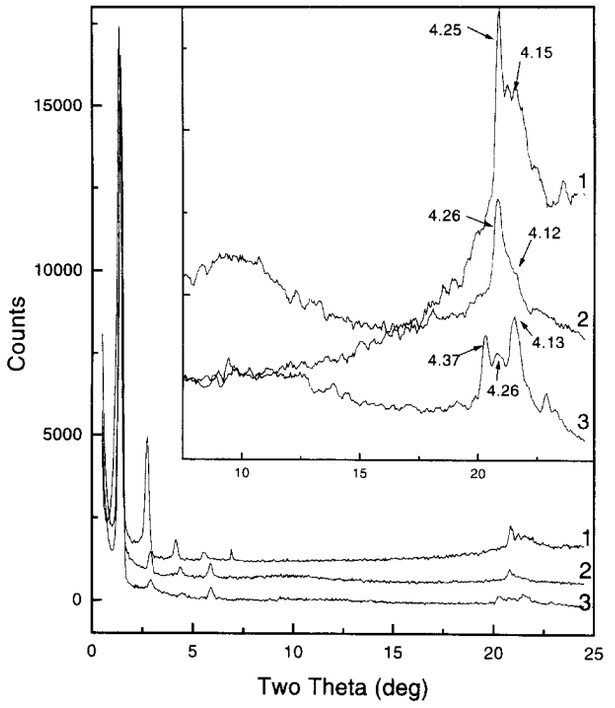

Fig. 10. Gel phase XRD spectra of DPPC samples taken after melting the subgel at the following DMSO/water mole fractions X and temperatures: (1) $X = 0$, 20°C; (2) $X = 0.16$, 38°C; (3) $X = 0.20$, 38°C. Spectra are offset along the vertical axis for clarity.

except for a very broad peak centered at 10° in the medium-angle region. Despite this difference, we will call this the normal G phase. However, spectrum 3 shows a strikingly different gel phase pattern in the wide-angle region for the $X = 0.20$ sample at 38°C. We will call this the G_S phase.

The ripple phase was observed for $X = 0$, 0.038 and 0.10 and Fig. 11 shows typical spectra. The low-angle D-spacing at 38°C in spectrum 1 is 69.7 Å, nearly the same as in spectrum 2 (69.5 Å at 43°C). The wide-angle pattern consists of only a single peak near 4.25 Å which is one characteristic that distinguishes the ripple phase from gel phases. Another characteristic showing that this is the ripple phase is the broad low-angle scattering features. With higher resolution these apparently broad peaks have been resolved into many peaks that are indexed to both the ripple repeat as well as the usual lamellar repeat [61]. At low resolution, these many peaks appear as in Fig. 11. Fig. 12 shows fluid phase spectra taken at 51°C. Hydrocarbon chain disorder is indicated by the absence of well-defined peaks in the wide-angle region at all X. The inset shows the low-angle region from $h = 2$ to $h = 4$, with more detectable orders of diffraction occurring at higher mole fractions of DMSO. As X increases, the interlamellar D-spacing decreases (Table 1).

In the $X = 0.20$ sample, phase coexistence of the fluid phase with lamellar D-spacing 54 Å and the gel phase with D-spacing 60 Å was evident as the temperature was decreased from 49 to 48°C, where the D-spacings 55 and 61 Å were both present. When $X > 0$, the Gibbs phase rule allows such phase coexistence because there are three molecular species instead of just two as for $X = 0$. At the lower concentrations two separate D-spacings could not be distinguished, so coexistence of lipid bilayer phases appears only in small temperature ranges.

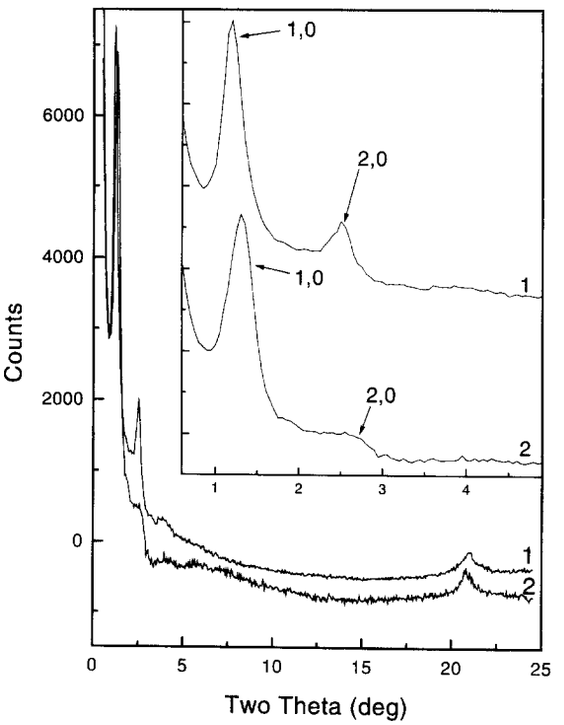

Fig. 11. Ripple phase XRD scans of DPPC at the following DMSO/water mole fractions X and temperatures: (1) $X = 0$, 38°C; (2) $X = 0.10$, 43°C. Spectra are offset along the vertical axis for clarity.

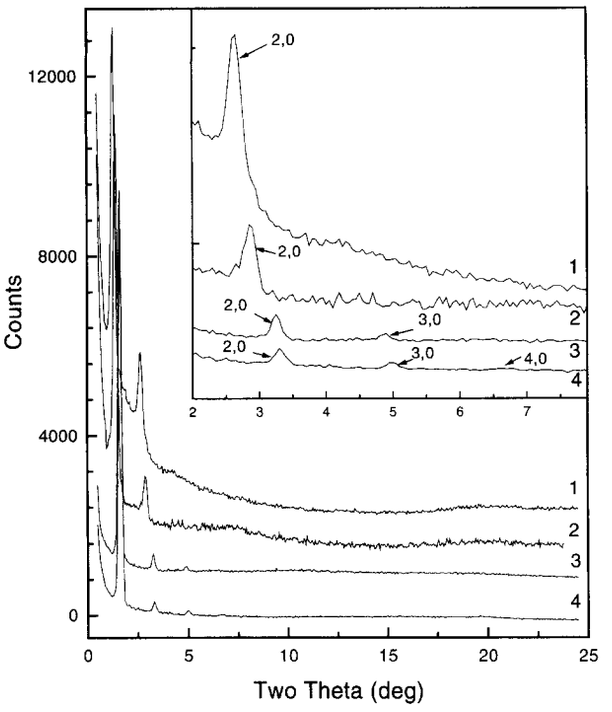

Fig. 12. Fluid phase XRD scans at 51°C of (1) $X = 0$; (2) $X = 0.10$; (3) $X = 0.16$; (4) $X = 0.20$. Spectra are offset along the vertical axis for clarity.

3.3. Electron density profiles

Fig. 13 shows the electron density profiles obtained for the subgel phases at 5-mol fractions X of DMSO. Although electron density profiles that employ only four or five orders of diffraction have low spatial resolution, the location of the headgroup peak is a fairly robust feature [31,62]. Fig. 13 shows that the new S subgel phase ($X = 0.20$) has a larger bilayer thickness than the usual C subgel phase ($X = 0$ and 0.038) by about 4 Å (see Table 1).

Fig. 14 shows electron density profiles for the gel phase. We wished to compare gel phase structures of samples with different X at the same temperature. This was accomplished by raising the temperature first to 51°C and then returning to 20°C. Even though the S phase is the stable phase at 20°C for samples with $X \geq 0.10$, the subgel phases do not nucleate unless the samples are taken to lower temperatures. Fig. 14 shows that there is no change in the head-to-head spacing with increasing mole fraction of DMSO. The average D_{HH} of the profiles in Fig. 14 is 44.2 ± 0.1 Å.

Reliable electron density profiles of the ripple

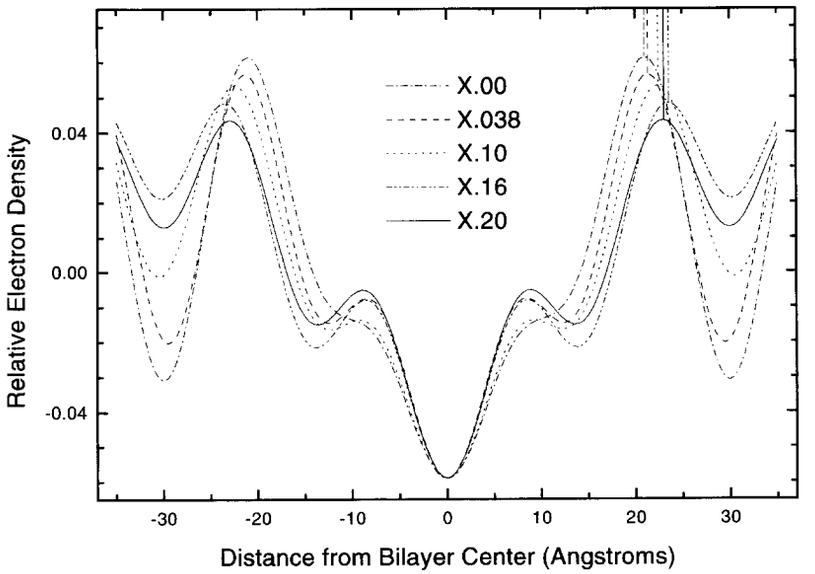

Fig. 13. Subgel phase electron density profiles at the following mole fractions X and temperatures: $X = 0$, 10°C; $X = 0.038$, 10°C; $X = 0.10$, 20°C; $X = 0.16$, 10°C; $X = 0.20$, 10°C. Vertical lines indicate positions of headgroup peaks.

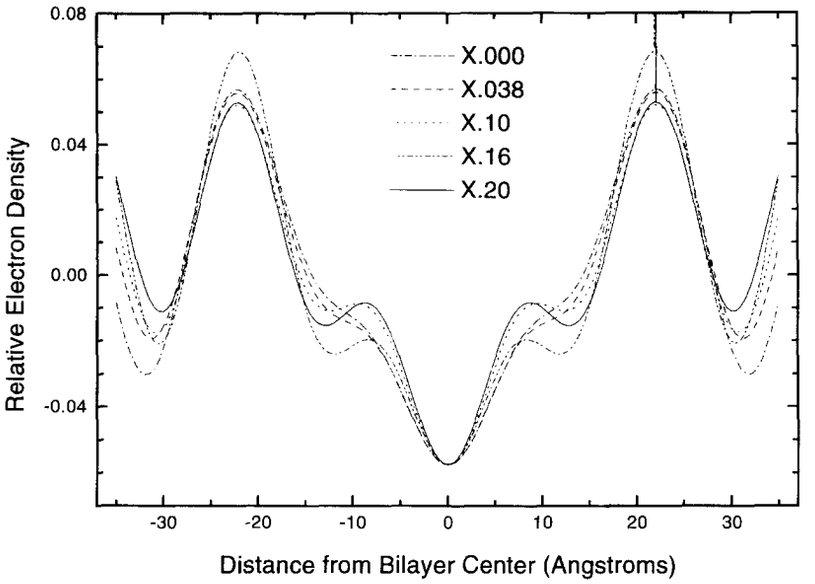

Fig. 14. Gel phase electron density profiles at 20°C. Vertical lines indicate positions of headgroup peaks.

phase were not possible due to the low resolution of these data. Fluid phase profiles (not shown) were calculated from X-ray data collected at 51°C. Even though the headgroup position is not well defined due to the small number of orders in the data, there is no evidence of change in head-to-head spacing D_{HH} as X is varied (see Table 1). The average D_{HH} is 38.7 ± 1.5 Å, which is consistent with the value determined for fully hydrated DPPC [62]. Following the convention of McIntosh et al. [63], we will add 10 Å to D_{HH} to obtain D'_B, which is a measure of the total bilayer thickness including the cholines. Subtracting D'_B from the D spacing then gives D'_W, which is a measure of the exclusive water thickness between neighboring bilayers. These values are summarized in Table 1 and show that the water thickness decreases with increasing X in the fluid phase.

4. Discussion

We have employed DSC and equilibrium XRD to explore the phase diagram of DPPC in solvent composed of X mole fraction of DMSO/water. A rough phase diagram is shown in Fig. 3. We note that the dashed lines that approximate the phase boundaries should really be two-phase regions, as verified by results at $X = 0.20$ and as allowed by the Gibbs phase rule, but apparently the DMSO/water solvent mixture between the bilayers does not deviate sufficiently from ideality to make these two-phase regions very large along the temperature axis. DSC is a relatively quick and easy technique that has been previously used to study these systems [43]. In addition to confirming many of the previous results, in our hands DSC strongly indicates the existence of a new S subgel phase for $X \geq 0.10$, which we subsequently confirmed with equilibrium XRD (Fig. 9).

4.1. Subgel phase

Interpretation of DSC results for equilibrium subgel phase transitions is complicated by the relatively slow kinetics of the phase transformations compared to the scanning rate of the DSC. Even though we used lower scanning rates (12–14°C/h) than previous DSC studies of DPPC in DMSO/water [43], the temperatures of the subgel peaks are greater than the true equilibrium transition temperatures. Interpretation of DSC is also complicated by the multiple subgel peaks whose appearance depends upon the time and temperature of incubation. However, only two principle subgel XRD spectra were obtained (spectra 1 and 3 in Fig. 9), indicating that the C^* and S^* DSC peaks (Figs. 1 and 2 and 4–6) are due to melting domain impacted phases rather than melting

a genuinely new subgel phase. In contrast, the *S* peaks in the DSC (Figs. 6 and 7) are associated with the formation of the new XRD subgel spectrum at $X = 0.16$ and 0.20.

Although DSC is not as conclusive as XRD regarding equilibrium phases, it is a convenient method to study kinetic effects of DMSO on subgel formation. At the lowest mole fraction of DMSO ($X = 0.038$) normal *C* subgel formation in DPPC was four times slower than in pure water, but the kinetics of *C* subgel formation became faster again as *X* increased. These results can be correlated to the picture of DMSO/water mixtures [64]. At low concentrations, ($X = 0.03$) DMSO acts as a kosmotrope [64,65] (water structure maker), which rigidifies water structure and might, therefore, be expected to slow the kinetics of headgroup ordering that is thought to be an essential feature of the subgel phase [50]. At higher concentrations, however, DMSO acts as a chaotrope [64,65] (water structure breaker), and might, therefore, be expected to increase the kinetics of headgroup reorientation and subgel formation, as observed. For $X \geq 0.10$, the *C* phase is metastable with respect to the slower forming new *S* subgel phase and the kinetics of *S* formation increase with increasing *X*, taking relatively short time of 27 days at $X = 0.20$. This is again consistent with the combined ideas that headgroup ordering is a key feature of subgel phases and that the more chaotropic nature of the solvent speeds headgroup kinetics. Also, a rotation of the headgroup may be required for efficient rearrangement of more highly crystalline chains expected in more condensed subgel phases.

Turning from kinetics to equilibrium, the enthalpy of melting of the *S* phase (9.5 kcal/mol) is much larger than the *C* subtransition enthalpy (4.5 kcal/mol) or even the main transition enthalpy (8.0 kcal/mol), thus indicating that the *S* subgel phase is a state of low enthalpy and entropy. In a Fourier-transform infrared study, Lewis and McElhaney [66] suggested that the driving force for *C* subgel formation in *n*-saturated diacylphosphatidylcholines is the formation of an extended hydrogen-bonding network in the interfacial region and that the optimization of this network probably requires some distortion of the optimal packing of the acyl chains. The present work supports this idea, since when the hydrogen-bonding network is broken up by DMSO, the *C* subgel phase ceases to be the most stable and the lower energy *S* subgel with more ideal chain packing can form.

A recent study of the ordinary *C* subgel phase of DPPC for $X = 0$ [50] succeeded in indexing the XRD peaks from oriented samples using models that involve headgroup ordering to explain the intermediate-angle peaks. Several different molecular arrangements within the headgroup unit cell remain possible in that analysis. Their model [50] does not involve inequivalence of the hydrocarbon chains (such as occurs in the herring-bone structure of crystalline alkanes) that is often invoked to explain the difference between the gel phase and the subgel phase. Our XRD data for unoriented powder samples of the *C* phase continue to agree with the previous data, but our data are clearly insufficient to resolve remaining uncertainties in the *C* phase structure. Similarly, our *S* phase data are insufficient to attempt a detailed structure of this phase. However, within the framework of the previous analysis [50], it appears that we can conclude that the quite different intermediate-angle pattern in the *S* phase (Fig. 9) indicates different headgroup ordering. From the low-angle data, we find that head-to-head thickness D_{HH} of the *S* phase is about 4 Å larger than for the *C* phase. This increase in D_{HH} could easily be accounted for by a decrease in chain tilt angle from 34.5° in the *C* phase to about 20° in the *S* phase.

It is interesting to compare the present results with another subgel investigation of pure DPPC, that of McIntosh and Simon [55], which used osmotic pressure to dehydrate the subgel and gel phases of DPPC. These authors found that the head-to-head spacing D_{HH} in the subgel phase did not change as a function of osmotic pressure, even down to $D'_W = 3$ Å, although at this small water space steric interactions between the headgroups from opposing bilayers began to be evident. Therefore, removal of water alone does not disturb the subgel structure which is largely determined by its hydrogen bonding to the remaining aqueous phase. Indeed, Kodama [67] has evidence that *C* subgel formation occurs when there are only 5 water molecules/PC headgroup and that the water at the headgroup is tightly bound. In our study, D'_W spacings close to 4 Å are seen at $X = 0.16$ and 0.20 in the subgel phase, with somewhat larger D'_W in the fluid and gel phases at these mole fractions (see Table 1). Thus, DMSO, like the polymer polyvinyl-

pyrrolidine (PVP), is able to extract water from the fluid space almost to the same extent as high osmotic pressure. One hypothesis to account for this would be that DMSO is excluded from the interlamellar space and, therefore, exerts a simple osmotic pressure on the MLVs. However, DMSO has a second important effect, namely, it changes the structure of the subgel phase. This proves that DMSO enters the interlamellar space and does not act just as a dehydrating agent. Of course, there could still be partial partitioning of the DMSO between the bulk and the interlamellar water as appears to occur for other solutes [68].

4.2. Gel phase

Turning now to the gel phase, our results for X less than 0.16 differ somewhat from the results of Yu and Quinn [43]. They reported that the DPPC bilayer thickness, as measured by the head-to-head spacing D_{HH} in electron density profiles, increased from 41.3 Å for $X = 0$ to 43.5 Å for $X = 0.11$, whereas in the present study (Table 1), we find gel phase D_{HH} to be 44.2 ± 0.1 Å and unaffected by DMSO. Our current value of D_{HH} agrees with previous values for $X = 0$ from our laboratory [56]. The largest error in calculating the electron densities may arise from the background subtraction or from the number of orders used for the profile. In order to test the background error, we subtracted the background intensity with the Microcal Origin software using three different techniques, and found no effect on the headgroup peak position. Also, the use of four orders has been shown to give profiles comparable to those obtained with 10 orders of diffraction [62], so we are confident that DMSO does not change the bilayer thickness or, by implication, the angle of chain tilt. Since the pretransition temperature does change with X, this suggests that the effect of DMSO is greater on the ripple phase than on the gel phase. However, DMSO does have an important effect on the water spacing of the gel phase, as previously noted by Yu and Quinn [43]. As can be seen from Table 1, increasing DMSO removes water from the interlamellar space in the gel phase.

For higher concentrations of DMSO, not previously studied in [43], our XRD reports a substantially different gel phase, named G_S in Fig. 3, that is clearly different from the usual gel phase at lower X. The usual gel phase in phosphatidylcholines has been well characterized for many years as essentially all-trans chains ordered on an orthorhombic (pseudo-hexagonal) lattice with each chain tilted close to nearest neighbors [2,69]. This gives rise to a sharp (20) peak and a broad (11) shoulder as seen in the wide-angle spectra 1 and 2 in Fig. 10. In contrast, spectrum 3 in Fig. 10 shows a three peak pattern in the wide angle region. Three peak patterns have been shown to occur in partially dehydrated DMPC and the resulting phase was called the $L_{\beta L}$ phase in contrast to the usual gel phase which was called the β I phase [70]. The essential difference in these two phases is that the direction of the chain tilt rotates from towards nearest neighbors in $L_{\beta I}$ to a general angle (neither towards nor directly between nearest neighbors) in the $L_{\beta L}$ phase. Since one effect of DMSO is to dehydrate the multilamellar vesicles, it seems reasonable that our new G_S might also be an $L_{\beta L}$ phase, although more careful study at higher instrumental resolution on oriented samples would be required to confirm this identification.

4.3. Ripple phase

Turning to the ripple phase, it was not possible in these studies to obtain the very high resolution spectra [61] that are necessary to elucidate the detailed structure of the ripple phase such as was recently obtained [71]. However, we have added to the study of the effect of DMSO on the stability of the ripple phase begun by Yu and Quinn [43]. They observed the loss of the pretransition by $X = 0.05$ in their heating scan and by $X = 0.11$ in the cooling scan. In our Figs. 5 and 11, we see evidence both calorimetrically and by X-ray diffraction for a ripple phase at $X = 0.10$ and for no ripple phase at $X = 0.16$. The loss of the pretransition in [43] in the heating scan is most likely due to the fast scan rate (300°C/h) compared to 13°C/h in our work; when we scanned an $X = 0.10$ sample at 60°C/h, we also did not observe a pretransition (data not shown). However, there is agreement that the major effect of increasing DMSO is to destabilize the ripple phase until it disappears. Indeed, it has been observed that the ripple phase does not exist below 17% water [67], and if full hydration is at 25% in the gel phase [72],

then loss of $\sim 1/3$ of the total water results in loss of the ripple phase. Similarly, D'_W decreases from 9.6 Å for $X = 0$ to 6.1 Å for $X = 0.16$ when the ripple phase disappears which again corresponds to loss of about $1/3$ of the original water. Therefore, it is plausible that the major effect of DMSO on the stability of the ripple phase is through dehydration.

4.4. Fluid phase

Our electron density profiles for the high temperature F (liquid-crystalline, L_α) phase are not very accurate because there are only a few orders of diffraction. However, the rough results for the fluid phase shown in Table 1 are consistent with the results for the lower temperature phases, namely, that DMSO dehydrates the interlamellar space. Also, our result that the main phase transition temperature T_m increases with increasing X agrees with earlier work [43]. As shown in Fig. 3, T_m increases from 41.4 to 46°C when X increases from 0 to 0.20. A similar increase in T_m occurs when DPPC bilayers lose nearly $3/4$ of the water of fully hydrated fluid phase lipid [73,67]. This is close to the water loss in the fluid phase with increasing DMSO as indicated by the change in D'_W in Table 1. From this alone one might conclude that it is the dehydration effect of DMSO that is primarily responsible for the increase in T_m, but this may be misleading for the following reason. With no DMSO the increase in T_m is highly non-linear with decreasing water content [67], but with DMSO T_m increases nearly linearly and D'_W decreases nearly linearly. Therefore, we conclude that, while DMSO has a generally dehydrating effect, there are also more specific solvent interactions with the lipid headgroups that affect the main transition. Such specific interactions must also be involved in the genesis of the new subgel phase found in this work.

This research was supported by US National Institutes of Health Grant GM44976.

References

[1] W.-J. Sun, S. Tristram-Nagle, R.M. Suter, J.F. Nagle, Biophys. J. 71 (1996) 885–891.
[2] S. Tristram-Nagle, R. Zhang, R.M. Suter, C.R. Worthington, W.-J. Sun, J.F. Nagle, Biophys. J. 64 (1993) 1097–1109.
[3] R.G. Snyder, G.L. Liang, H.L. Strauss, Biophys. J. 71 (1996) 3186–3198.
[4] W.-J. Sun, S. Tristram-Nagle, R.M. Suter, J.F. Nagle, Biochim. Biophys. Acta 1279 (1996) 17–24.
[5] K.H. Cheng, P. Somerharju, Biophys. J. 70 (1996) 2287–2298.
[6] F. Separovic, K. Gawrisch, Biophys. J. 71 (1996) 274–282.
[7] R.N.A.H. Lewis, R.N. McElhaney, F. Osterberg, S.M. Gruner, Biophys. J. 66 (1994) 207–216.
[8] S. Li, Z.-q. Wang, H.-n. Lin, C. Huang, Biophys. J. 65 (1993) 1415–1428.
[9] E.N. Serrallach, G.H. deHaas, Shipley, G.G. 23 (1984) 713–720.
[10] C.P. Yang, M.C. Wiener, R.N.A.H. Lewis, R.N. McElhaney, J.F. Nagle, Biochim. Biophys. Acta 863 (1986) 33.
[11] D.A. Mannock, R.N.A.H. Lewis, R.N. McElhaney, M. Akiyama, H. Yamada, D.C. Turner, S.M. Gruner, Biophys. J. 63 (1992) 1355–1368.
[12] P. Laggner, K. Lohner, G. Degovics, K. Muller, A. Schuster, Chem. Phys. of Lipids 44 (1987) 31–60.
[13] R.N.A.H. Lewis, W. Pohle, R.N. McElhaney, Biophys. J. 70 (1996) 2736–2746.
[14] P.M. Brown, J. Steers, S.W. Hui, P.L. Yeagle, Silvius, J.R. 25 (1986) 4259–4267.
[15] J. Gagne, L. Stamatatos, T. Diacovo, S.W. Hui, P.L. Yeagle, J. Silvius, Biochemistry 24 (1985) 4400–4408.
[16] S.M. Gruner, M.W. Tate, G.L. Kirk, P.T.C. So, D.C. Turner, D.T. Keane, C.P.S. Tilcock, P.R. Cullis, Biochemistry 27 (1988) 2853–2866.
[17] Y.K. Levine, Prog. Surface Sci. 3 (1973) 279–352.
[18] V.A. Parsegian, N. Fuller, R.P. Rand, Proc. Natl. Acad. Sci. USA 76 (1979) 2750–2754.
[19] S.A. Simon, T.J. McIntosh, Proc. Natl. Acad. Sci. USA 86 (1989) 9263–9267.
[20] B. Bonev, M.R. Morrow, Biophys. J. 70 (1996) 2727–2735.
[21] L.F. Braganza, D.L. Worcester, Biochemistry 25 (1986) 2591–2595.
[22] M. Lafleur, M. Bloom, E.F. Eikenberry, S.M. Gruner, Y. Han, P.R. Cullis, Biophys. J. 70 (1996) 2747–2757.
[23] D.C. Turner, S.M. Gruner, Biochemistry, 31 (1992)
[24] G. Cevc, J.M. Seddon, R. Hartung, W. Eggert, Biochim. Biophys. Acta 940 (1988) 219–240.
[25] H. Takahashi, T. Yasue, K. Ohki, I. Hatta, Phase Transitions 45 (1993) 157.
[26] B.A. Cunningham, L.J. Lis, Biochim. Biophys. Acta 861 (1986) 237–242.
[27] H. Hauser, K. Howell, FEBS Letts. 80 (1977) 355–359.
[28] G.L. Jendrasiak, R. Smith, A.A. Ribeiro, Biochim. Biophys. Acta 1145 (1993) 25–32.
[29] L.J. Lis, V.A. Parsegian, R.P. Rand, Biochemistry 20 (1981) 1761–1770.
[30] R.V. McDaniel, S.A. Simon, T.J. McIntosh, Biochim. Biophys. Acta 731 (1983) 97–108.
[31] T.J. McIntosh, A.D. Magid, S.A. Simon, Biochemistry 28 (1989) 7904–7912.

[32] C.W.N. Cumper, S. Walker, Trans. Faraday Soc. 52 (1956) 193–199.
[33] Weast (Ed.), CRC Handbook of Chemistry and Physics, CRC Press, Inc., Boca Raton, Florida, 1980, pp. E64.
[34] D. Martin, H.G. Hauthal, Dimethyl-Sulphoxide, Van Nostrand Reinhold, 1971.
[35] A. Luzar, J. Chem. Phys. 91 (1989) 3603–3613.
[36] J. Ali, J.N. Shelton, J. Reprod. Fertil. 99 (1993) 471–477.
[37] W.O. Gross, Z. Naturforsch. B 23 (1968) 512–519.
[38] J.E. Lovelock, M.W.H. Bishop, Nature (London) 183 (1959) 1394.
[39] R.K. Mahajan, D.M. Renapurkan, J. Helminthol. 67 (1993) 233–237.
[40] L.M. Crowe, J.H. Crowe, Biochim. Biophys. Acta 946 (1988) 193–201.
[41] J.H. Crowe, L.M. Crowe, D. Chapman, Science 223 (1984) 701–703.
[42] W. Curatolo, Biochim. Biophys. Acta 817 (1985) 134–138.
[43] Q.-W. Yu, P.J. Quinn, Biophys. J. 69 (1995) 1456–1463.
[44] S.E. Church, D.J. Griffiths, R.N.A.H. Lewis, R.N. McElhaney, H.H. Wickman, Biophys. J. 49 (1986) 597–605.
[45] L. Finegold, M.A. Singer, Chem. Phys. Lipids 35 (1984) 291–297.
[46] R.N.A.H. Lewis, R.N. McElhaney, Biophys. J. 61 (1992) 63–77.
[47] R.N.A.H. Lewis, N. Mak, R.N. McElhaney, Biochemistry 26 (1987) 6118–6126.
[48] S. Tristram-Nagle, M.C. Wiener, C.-P. Yang, J.F. Nagle, Biochemistry 26 (1987) 4288–4294.
[49] S.C. Chen, J.M. Sturtevant, B.J. Gaffney, Proc. Natl. Acad. Sci. USA 77 (1980) 5060–5063.
[50] J. Katsaras, V.A. Raghunathan, E.J. Dufourcq, J. Dufourcq, Biochemistry 34 (1995) 4684–4688.
[51] S. Tristram-Nagle, R.M. Suter, W.-J. Sun, J.F. Nagle, Biochim. Biophys. Acta 1191 (1994) 14–20.
[52] M. Akiyama, J. Appl. Phys. (Japan) 24 (1985) 231–234.
[53] M. Akiyama, N. Matsushima, Y. Terayama, J. Appl. Phys. (Japan) 26 (1987) 1587–1591.
[54] M.J. Ruocco, G.G. Shipley, Biochem. Biophys. Acta 691 (1982) 309–320.
[55] T.J. McIntosh, S.A. Simon, Biochemistry 32 (1993) 8374–8384.
[56] M.C. Wiener, R.M. Suter, J.F. Nagle, Biophys. J. 55 (1989) 315–325.
[57] C.P. Yang, J.F. Nagle, Phys. Rev. A 37 (1988) 3993–4000.
[58] J.F. Nagle, D.A. Wilkinson, Biochemistry 21 (1982) 3817–3821.
[59] M. Kodama, M. Kuwabara, S. Seki, BBA 689 (1982) 567–570.
[60] D.A. Wilkinson, J.F. Nagle, Biochemistry 23 (1984) 1538–1541.
[61] D.C. Wack, W.W. Webb, Phys. Rev. A 40 (1989) 2712.
[62] J.F. Nagle, R. Zhang, S. Tristram-Nagle, W. Sun, H.I. Petrache, R.M. Suter, Biophys. J. 70 (1996) 1419–1431.
[63] T.J. McIntosh, A.D. Magid, S.A. Simon, Biochemistry 26 (1987) 7325–7332.
[64] Q.-W. Yu, P.J. Quinn, Bioscience Reports 14 (1994) 259–281.
[65] I.I. Vaisman, M.L. Berkowitz, J. Am. Chem. Soc. 114 (1992) 7889–7896.
[66] R.N.A.H. Lewis, R.N. McElhaney, Biochemistry 29 (1990) 7946–7953.
[67] M. Kodama, Thermochimica Acta 109 (1986) 81–89.
[68] S.M. Gruner, R.P. Lenk, A.S. Janoff, M.J. Ostro, Biochemistry 24 (1985) 2833–2842.
[69] W.-J. Sun, R.M. Suter, M.A. Knewtson, C.R. Worthington, S. Tristram-Nagle, R. Zhang, J.F. Nagle, Phys. Rev. E 49 (1994) 4665.
[70] G.S. Smith, E.B. Sirota, C.R. Safinya, R.J. Plano, N.A. Clark, J. Chem. Phys. 92 (1990) 4519–4529.
[71] W.-J. Sun, S. Tristram-Nagle, R.M. Suter, J. F Nagle, Proc. Natl. Acad. Sci. USA 93 (1996) 7008–7012.
[72] M.J. Janiak, D.M. Small, G.G. Shipley, Biochemistry 15 (1976) 4575–4580.
[73] D. Chapman, R.M. Williams, B.D. Ladbrooke, Chem. Phys. Lipids 1 (1967) 445–475.
[74] M.C. Wiener, S. Tristram-Nagle, D.A. Wilkinson, L.E. Campbell, J.F. Nagle, Biochim. Biophys. Acta 938 (1988) 135–142.